ELSEVIER

NeuroImage

www.elsevier.com/locate/ynimg
NeuroImage 21 (2004) 876–885

Spatial relationship between neuronal activity and BOLD functional MRI

Dae-Shik Kim,[a,b,*] Itamar Ronen,[a,b] Cheryl Olman,[a] Seong-Gi Kim,[a,1] Kamil Ugurbil,[a] and Louis J. Toth[a,b]

[a] *Center for Magnetic Resonance Research, University of Minnesota Medical School, Minneapolis, MN 55455, USA*
[b] *Department of Anatomy and Neurobiology, Boston University School of Medicine, Boston, MA 02118, USA*

Received 21 May 2003; revised 7 October 2003; accepted 14 October 2003

Despite the ubiquitous use of functional magnetic resonance imaging (fMRI), the extent to which the magnitude and spatial scale of the fMRI signal correlates with neuronal activity is poorly understood. In this study, we directly compared single and multiunit neuronal activity with blood oxygenation level-dependent (BOLD) fMRI responses across a large area of the cat area 18. Our data suggest that at the scale of several millimeters, the BOLD contrast correlates linearly with the underlying neuronal activity. At the level of individual electrode recording sites, however, the correlation between the two signals varied substantially. We conclude from our study that T_2*-based positive BOLD signals are a robust predictor for neuronal activity only at supra-millimeter spatial scales.

Keywords: BOLD; Neuronal activity; fMRI

Introduction

Since its introduction in 1992 (Bandettini et al., 1992; Kwong et al., 1992; Ogawa et al., 1992) blood oxygenation level-dependent (BOLD) functional magnetic resonance imaging (fMRI) has revolutionized cognitive neurosciences by allowing the foci of cortical "activity" to be visualized in vivo in a noninvasive manner. The BOLD contrast originates from the intravoxel magnetic field inhomogeneity induced by paramagnetic deoxyhemoglobin (deoxyHb) sequestered in red blood cells that are compartmentalized within blood vessels. The magnetic susceptibility differences between the deoxyHb-containing compartments and the surrounding space generate magnetic field gradients around the boundaries of these compartments. Therefore, perturbation of regional deoxyHb content will alter the signal intensities in MR images sensitized to BOLD contrast. Such regional perturbation occurs as the result of enhanced neuronal activity and metabolism during sensory (Engel et al., 1994), motor (Kim et al., 1993), or cognitive (Wagner et al., 1998) functions.

While BOLD-based neuroimaging studies have provided unprecedented amount of insights into the workings of the human brain in vivo, the explanatory power of BOLD fMRI is currently limited since there is a fundamental gap in our understanding of the linkage between the observed BOLD contrast and the underlying neuronal physiology. In particular, the extent to which the magnitude and spatial scale of the BOLD signal correlates with neuronal physiology remains elusive (Attwell and Iadecola, 2002; Ugurbil et al., 2003) To this end, a growing body of results suggests a predominantly linear coupling between BOLD and neuronal activity. For example, a recent study by Ogawa et al. (2000) demonstrated a linear relationship between somatosensory-evoked potentials and BOLD signals for brief stimulation durations. Rees et al. (2000) and Heeger et al. (2000) demonstrated a linear correlation between BOLD contrast in humans and averaged spike rate in a monkey cortical area during stimulation with nearly identical stimuli. A similarly linear relationship was observed also in anesthetized monkeys by Logothetis et al. (2001), a study in which single-unit responses were acquired simultaneously with BOLD signals inside the MRI scanner.

While the above results suggest that the fundamental coupling between BOLD and the underlying neuronal activity is approximately linear, important questions remain about the spatial scale over which the linear coupling remains valid. Is the hypothesized linear coupling between BOLD and neuronal activity invariant across the different spatial scales of the cortical architecture? Can we assume a universal linearity from the spatial scale of entire cortical areas (several millimeters to centimeters) to individual cortical columns (sub-millimeter)? Such universal linearity would be surprising, since the BOLD signal is not a direct measure of neuronal activity per se. Rather, it is a complex convolution of changes in cerebral metabolic rate of oxygen ($CMRO_2$), cerebral blood flow (CBF), and cerebral blood volume (CBV) following focal neuronal activity. Therefore, spatial specificity of BOLD response becomes a critical issue in examining its relationship to the underlying neuronal activity. It is in principle possible to record from a site where

* Corresponding author. Department of Anatomy and Neurobiology, Boston University School of Medicine, 715 Albany St., Boston, MA 02118.
E-mail address: dskim@bu.edu (D.-S. Kim).
[1] Present address: University of Pittsburgh, Pittsburgh, PA, USA.
Available online on ScienceDirect (www.sciencedirect.com.)

1053-8119/$ - see front matter © 2004 Elsevier Inc. All rights reserved.
doi:10.1016/j.neuroimage.2003.10.018

neuronal activity is absent but there exists a large BOLD response as the latter effect "spills over" from an adjacent active region due to lack of spatial specificity. Consequently, it cannot be assumed a priori that the correlation between the BOLD signals and the underlying neural activity is linear irrespective of spatial considerations, especially at the sub-millimeter scale at which the finest details of spatial organization in cortex have been observed.

In the present study, we utilize a novel recording scheme to characterize the relationship between BOLD fMRI signals and the underlying neuronal modulation within the same animals from multiple electrode recording sites over a large cortical area. Our study extends recent results (Logothetis et al., 2001) in which correlations between BOLD and neuronal activity were characterized from a single electrode penetration site. With multiple recording sites spaced over the entire cat area 18 on the lateral gyrus, the results of our study provide a detailed look into the spatial relationship between neuronal activity and BOLD functional signals.

Materials and methods

Animal preparation

Juvenile cats between postnatal weeks 5 and 12 were used for the present studies. All procedures conformed to federal and state guidelines for treatment of animals and were approved by the University of Minnesota IACUC. Animals were initially anesthetized with ketamine (10–25 mg/kg, i.v.) and xylazine (2.5 mg/kg). The animals were intubated and artificially ventilated under isoflurane anesthesia (0.8–1.5%) in a N_2O/O_2 mixture of 70:30 throughout the experiment. Contact lenses were used to focus the retinal vasculature on the tangent screen using back-projection. The animal was placed in a cradle and restrained in normal postural position using a custom-designed stereotaxic frame. Foam earplugs (30 dB) were used to minimize exposure to gradient noise. End-tidal CO_2 (3.8–4.0%), respiration rate (25–35 strokes/min, 15–30 ml/stroke) and rectal temperature (37.5–38.0°C) were monitored throughout the experiment.

"Cartesian grid" implantation

Before MRI scans, the animal's visual cortex was exposed. A MR-transparent grid of Cilux (Crist Instruments, Maryland) and surface RF coil were mounted on the skull. Grid holes were filled with MR-opaque 2% agarose and imaged for precise registration of recording sites with the BOLD activity map. T_2*-based positive BOLD and single-unit responses were obtained in six hemispheres from three animals.

Stimulation paradigm

Animals were stimulated binocularly. Visual stimuli consisted of left–right moving high-contrast square-wave bidirectional gratings of vertical orientation and six different spatial frequencies (0.015, 0.047, 0.08, 0.15, 0.30, 0.47 and 0.81 cyc/deg, 2 cyc/s), covering the range of frequencies to which neurons in cat area 18 respond. During the baseline period, the upcoming stimulus was shown as a stationary grating. A video projector (Resonance Technology Co., California, resolution: 640 × 480 pixels) was used to project the visual stimuli onto a screen positioned 15 cm from the animal's eyes. The screen covered about 37° of the animal's visual field.

MR methods

All MR experiments were performed on a 4.7 T/31 cm (Oxford, UK) horizontal MRI scanners equipped with a 15 G/cm magnetic field gradients. BOLD measurements on a single image slice were made using the gradient-echo echo-planar imaging (EPI) technique. The imaging slice was positioned 500–700 μm below the pia mater to avoid superficial draining vessels. We calculated the potential spatial mismatch along the phase-encoded (PE) axis between the EPI image of the cortex and the FLASH image of the chamber by measuring the frequency difference between the two slices, and found a maximum theoretical misalignment of ±2 pixels. We therefore verified the image registration by shifting the EPI map by −2, −1, +1, and +2 pixels along the PE plane, and noting that the strongest correlations were obtained with zero shift. This suggests the FLASH and EPI images were properly in register. The MR imaging parameters were: data matrix = 64 × 64; single-shot EPI, FOV = 2 cm × 2 cm, slice thickness = 2 mm, TE/TR = 31 ms/0.5 s. Native in-plane resolution therefore was 312 μm. A total of 160 images were acquired during each epoch: 60 images before stimulation, 20 images during stimulation, and 80 images after stimulation. Images obtained for similar spatial frequencies were averaged for SNR improvement (usually 5–10 epochs). Collecting a robust negative BOLD signal would have required more averaging due to its inherently lower SNR. Therefore, to minimize the time to the single-unit recording phase, no attempt was made to analyze negative BOLD signals in these animals. Unless stated otherwise, percentage of BOLD modulation was calculated as (max − baseline) / baseline.

Single-unit recording

At the conclusion of the MR recording session, the animal was transferred to the neighboring physiological recording room. Control of anesthesia was maintained within the same limits necessary to achieve good hemodynamic signals. Projector and screen for visual stimuli were set up in an identical geometry as inside the magnet. Recording sites are selected from the entire region of exposed cortex, using an anatomical scan with superimposed grid as a guide to avoiding surface vasculature and areas of artifactual MR signal. Stimulus presentation and timing were kept identical to that used in the magnet except that the interstimulus interval was shortened from 30 s (for BOLD imaging) necessary for hemodynamic recovery to 10 s (for single-unit recording), more appropriate for single-unit recovery from adaptation. Initial single-unit recordings were done with both 10- and 30-s intervals to confirm that any difference in activity levels between these two states was within our experimental error. Each stimulus was presented 10 times and stimuli were interleaved. Single-unit activity was recorded with standard tungsten microelectrodes with a tip diameter of 5–7 μm and impedance of 2–4 MΩ, and amplified 10000× with standard equipment (Bak Electronics, Germantown, MD). The analog signal and stimulus sequence was recorded continuously (Power1401, Cambridge Electronics Design) allowing for off-line spike discrimination and filtering. Vertical penetrations through the grid were made using a hydraulic microdrive (Kopf, Tujunga, CA). Electrodes were advanced to approximately 200–400 μm below the cortical surface, and the first isolatable single unit found thereafter was recorded. For analysis, only one unit from each grid location was included. The entire craniotomy and chamber remained sealed with wax and agar at all times, and

electrodes were introduced through agar-filled guide holes. Between 1 and 3 cells were recorded from each penetration, and the cell with the best modulation used for analysis. Between 15 and 20 penetrations were conducted in each animal, requiring 12–15 h of recording. Neuronal signals were collected and stored as an analog waveform at 20 kHz. Peristimulus time histograms were generated for the spiking activity, collected using redundant on-line and off-line window discriminators, and for various frequency bands of the analog signal. Waveform power spectra were evaluated to determine which frequency bands were likely to contain the most information. Activity in pass bands of 0.3–0.7, 0.1–0.3, and 20–80 Hz was used to estimate neuronal activity over increasingly large areas around the electrode. The intention was to use the higher-frequency band as an estimate for multiunit activity of cells near the electrode tip (MUA), and the lower-frequency band as an approximation of the local field potential activity (LFP). Despite efforts to shield the recording setup from room noise, the 20–80 Hz band often contained significant power at 60 Hz, which required preprocessing with a digital band-stop filter.

Single-unit data analysis

Single-unit tuning curves for spatial frequency were constructed in analogous fashion to BOLD data by calculating (A − B) / B where B is the average baseline activity in spikes per second during the period 5 s before the onset of stimulus motion, and A is the average activity during stimulus motion. Average activity was calculated over 10 s of stimulus presentation. A similar calculation was made for the LFP and MUA data based on the levels (mV/s) of the filtered, rectified, and averaged analog signal.

Shuffling of BOLD single-unit pairs

Since the number of single-unit recording sites is much less than the number of voxels in the MR image, the following method was used to determine how many voxels need be averaged to obtain a reliable signal estimate: BOLD–single-unit data pairs from individual recording sites were shuffled using methods of Monte Carlo permutation. Correlations between n randomly shuffled single-unit sites and their corresponding n BOLD sites were calculated. The R^2 values for an exhaustively large population of random shufflings (10,000) were calculated at each value of n up to the maximum number of sites recorded, and plotted against the cortical area represented, calculated as square root of $n \times 900\ \mu m^2$ (cortical area within one sample point). Data were visualized as a probability plot of R^2 using logarithmic contours (since the actual probability is a function of bin size).

Results and discussion

It is known that across the surface of visual cortex, orientation and spatial frequency preferences change on a scale of hundreds of micrometers (Hubel and Wiesel, 1962; Hubener et al., 1997; Issa et al., 2000; Maffei and Fiorentini, 1977); therefore, it is necessary to co-register single-unit recordings and fMRI data within that level of precision. For such accurate registration that would allow the evaluation of both the *relationship between magnitudes of the* neuronal and fMRI signals and the *spatial dependence of this relationship*, a positioning method was designed for this study that is visible in MRI, does not introduce susceptibility artifacts to which GE-EPI is extremely sensitive, and is fully compatible with standard single-unit recording electrodes and hardware. Fig. 1 shows the details of the hardware (see Materials and methods for further details). Panel A shows a transmit–receive linear surface radiofrequency coil (RF coil) in which the nonmagnetic recording grid (“Cartesian recording grid”) has been embedded. The recording grid consists of 220 guide holes, where the distance between neighboring guide holes is 1 mm. Each of the 220 guide holes was then filled with 2% agarose gel in 0.9% saline solution, which provides excellent contrast in MR images, retaining the MRI properties of brain tissue. Before MRI scans, the animal’s visual cortex was exposed, and the Cartesian recording grid was mounted on the skull. Panel B of Fig. 1 displays the MR image of the recording chamber. Guide holes are clearly visible, while the recording chamber itself remains virtually invisible. The geometric arrangement of the 220 guide holes provided a coordinate system for the subsequent co-registration of the BOLD and single-unit data obtained from the same and identifiable cortical locations. Fig. 1C shows the side view of the RF coil with the embedded recording chamber before implantation. Panel D in Fig. 1 displays the AP3 coronal view of the cat visual cortex following the craniotomy, durotomy, and implantation of the recording chamber/RF coil.

Fig. 2A shows—on the coronal view of the cat visual cortex—the two axial slices acquired for functional studies: one tangential to the recording chamber (“chamber slice”), and the other one tangential to the cortical surface, targeting cortical layers II/III and IV, approximately 500–700 μm deep (“cortex slice”). The positions of the guide holes from the “chamber slice” could therefore be overlaid on the functional MRI map of the “cortex slice” (Fig. 2B). Each guide hole was aligned 3-D with the underlying anatomical and BOLD activation images. In summary, this technique allowed direct correlations between BOLD and single-unit data from a large number of independent recording sites across a large cortical area.

Combined BOLD and single/multiunit recording

Reliable BOLD signals could be obtained from cat area 18 after craniotomy, durotomy, and recording chamber implantation. Furthermore, the precise positions of the guide holes could be superimposed on the BOLD activation maps. Fig. 3 shows the result of a combined BOLD and single-unit recordings from the same cortical location. Here, the result from one particular cortical x–y location is depicted (a total of n = 58 BOLD–single-unit pairs from six hemispheres in three animals were obtained in this study). Identical visual stimuli were used for fMRI and subsequent single-unit recording sessions. As evident in Fig. 3, there is a marked difference between the kinetics of the observed BOLD signals and the underlying single-unit response. The neuronal response, as measured by summed spike rate, tightly follows the onset of stimulus presentation (indicated by the gray box in the background). Fig. 3 also shows a comparison of the time course of window-discriminated single-unit activity (blue peristimulus histogram) and multiunit activity filtered between 100 and 300 Hz (black trace) alongside the time course of the BOLD signal (red trace). Single-unit and multiunit activities follow similar time courses relative to the stimulus. The hemodynamic BOLD response on the other hand is not observed until 3–4 s after stimulus onset, as expected. In fact, a large fraction of the neuronal response is observed before any substantial BOLD hemodynamic response appears. The maximum BOLD response occurs around 10–15 s after stimulus onset, and is followed by a slow decline to baseline.

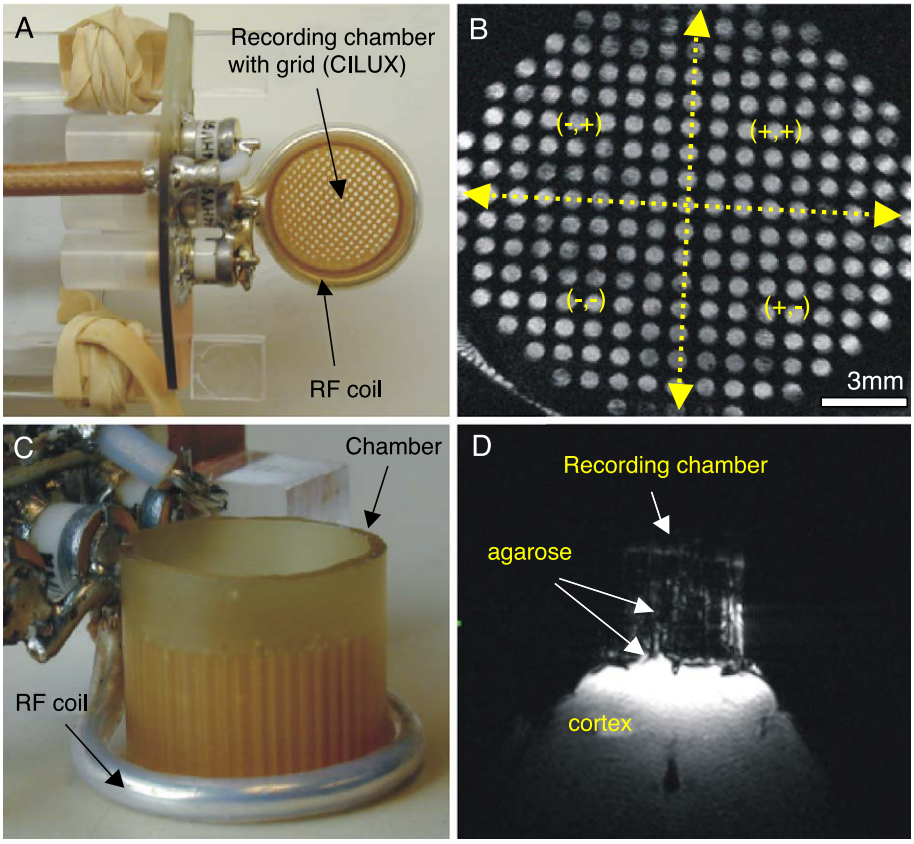

Fig. 1. Consecutive recording method for BOLD and single-unit correspondence. Panel A shows a top view of the transmit–receive linear surface radiofrequency coil (RF coil) in which the nonmagnetic recording grid ("Cartesian recording grid") has been embedded. Panel B displays the MR image of the recording chamber after it has been implanted atop the animal's visual cortex. Up: anterior; down: posterior; left: left; right: right. Panel C shows the side view of the RF coil with the embedded recording chamber before implantation. Panel D displays the coronal MRI of the recording grid implanted over the cat visual cortex following craniotomy and durotomy.

Fig. 2 shows that BOLD contrast can indicate a focal increase in neuronal activity over a large area, but not whether the finer spatial patterns of the BOLD signal also correlate with neuronal activity. Therefore, stimuli were chosen that would elicit spatially patterned responses on a variety of scales above that of the MRI voxel resolution. Spatial-frequency-modulated moving gratings of one orientation generated a spatial pattern of activity across the cortical surface due to the differential modulation of iso- and cross-orienta-

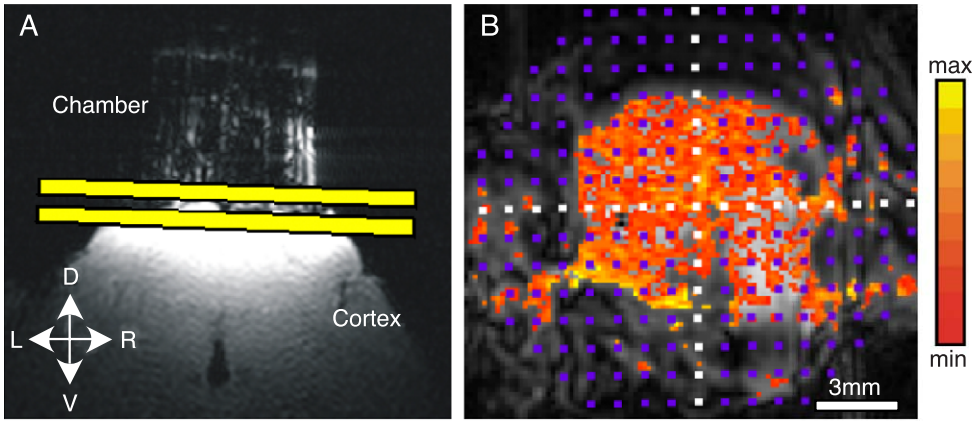

Fig. 2. Overlay of recording grid positions on the cat visual cortex. (A) The two axial slices acquired for functional studies are shown superimposed on the coronal anatomical section. One slice is tangential to the recording chamber, and the other tangential to the cortical surface, targeting cortical layers II/II and IV, approximately 500–700 μm deep. V: ventral; D: dorsal; L: left; R: right. (B) The positions of the guide holes overlaid on the functional MRI map. Up: anterior; down: posterior; left: left hemisphere; right: right hemisphere. The color key to the right of panel B indicates the cross-correlation coefficients used for functional image construction. Scale bars in panel B: 3 mm.

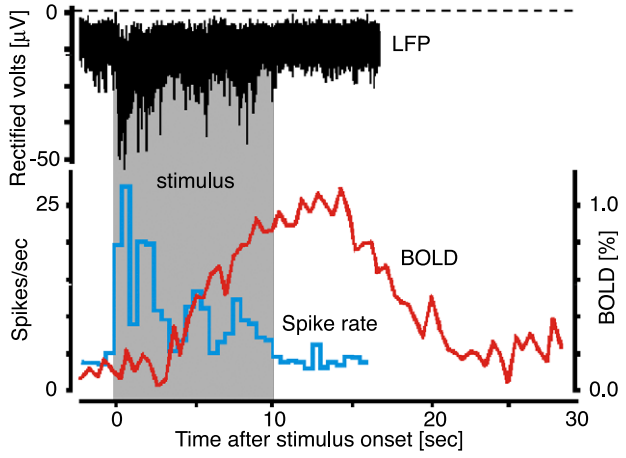

Fig. 3. Time course of BOLD and single-unit recordings from the same cortical location. Identical visual stimuli were used for fMRI and subsequent single-unit recording sessions. Blue trace: peristimulus histogram of the spike activity. Bin size for the histogram = 0.5 s = TR for fMRI. Red trace: percentage of BOLD changes during visual stimulation; *x*-axis: time after stimulus onset; left *y*-axis: spikes per second; right *y*-axis: percentage of BOLD changes; gray box: stimulus duration. The black trace above indicates the original low-frequency analog signals (100–300 Hz) underlying the depicted spike counts. See text for further details.

tion columns. Since previous attempts to distinguish orientation columns using the positive BOLD signal have been unsuccessful (Kim et al., 2000; Duong et al., 2001), it was necessary to generate patterned activation at a larger spatial scale. Distinguishing two iso-orientation sites from each other requires less resolution than distinguishing an iso- from a cross-orientation site. Furthermore, spatial frequency preference varies across visual cortex on a scale of millimeters (Issa et al., 2000). Therefore, spatial frequency was used to modulate activity at iso-orientation sites. Spatial frequency tuning curves were generated at each single-unit recording site for both the single-unit activity and the BOLD response. Such BOLD–single-unit pairs were obtained across a large area of the cat primary visual cortices (n = 58 pairs from six hemispheres). Six different spatial frequencies (0.015–0.81 cyc/deg, 2 cyc/s) were chosen to evoke a large dynamic range of response rates from cells in area 18 of cat visual cortex (Movshon et al., 1978). The response amplitudes for BOLD and the single-unit signals to each of the six frequencies were then directly compared using linear regression. Fig. 4 summarizes the results of such direct comparison across all sites. When data for all BOLD–single-unit pairs were averaged (n = 58 pairs), there were robust linear correlations between BOLD and single-unit measures of spatial frequency modulation over baseline (R^2 = 0.85). From the slope of the regression line, in this specific cortical area, using common values for BOLD signal parameters and using a typical visual stimulus condition, a 1% increase in observable BOLD signal reflects a modulation of about eight spikes per second.

Spikes or LFP?

This study was not designed to address whether BOLD signals correlate better with extracellular, intracellular, or presynaptic measures of neuronal activity. As it is generally agreed that neurons transfer information through the frequency of action potentials (Shadlen and Newsome, 1994; Singer, 1999), extracellular measures of spike rates have been considered the most relevant. In fact, the data suggest that the quality of correlation between BOLD and electrophysiological signals is largely invariant among different ways of measuring extracellular activity if BOLD–single-unit pairs are averaged from a sufficiently large area. As an example, the neuronal response was divided into transient (first 2 s) and sustained (final 8 s) components, and the linear regression was calculated between BOLD and bandpass-filtered neuronal responses representing MUA and LFP. For transient components, values of R^2 of 0.88 for single unit, 0.77 for MUA, and 0.78 for LFP were obtained. For the sustained component, values of 0.76 for single unit, 0.80 for MUA, and 0.81 for LFP were obtained. Importantly, the fact that these correlations are all very similar suggests that it is fair to use tuning curves derived from single units as representative of the tuning at each site.

Spatial correspondence between BOLD and neural activity

To address the question of spatial correspondence of the two measures, the correlation between BOLD and individual single-unit responses was calculated for individual recording sites. For each comparison, only BOLD responses from within the respective single-unit recording site were used. Signals were averaged from 3 × 3 voxels equivalent to an area of 900 × 900 μm. Fig. 5 displays typical tuning curves that were found. The right panel shows a tangential image of the cat area 18 following craniotomy and chamber implantation. The blue squares indicate the positions of the Cartesian guide holes. The numbered white squares stand for guide hole positions from which single-unit responses were obtained following the MRI session (n = 19 in this animal). The

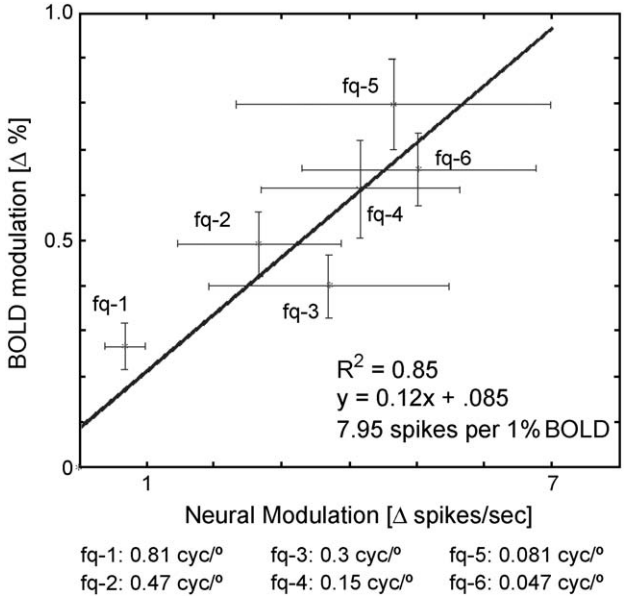

Fig. 4. Results of direct comparison between BOLD and single-unit recordings across all sites (n = 58). *x*-axis: neural modulation in spikes per second; *y*-axis: percentage of BOLD modulation. The data points fq-1 through fq-6 indicate the six spatial frequencies used to elicit neural responses. Coefficient of determination of the regression line R^2 = 0.85.

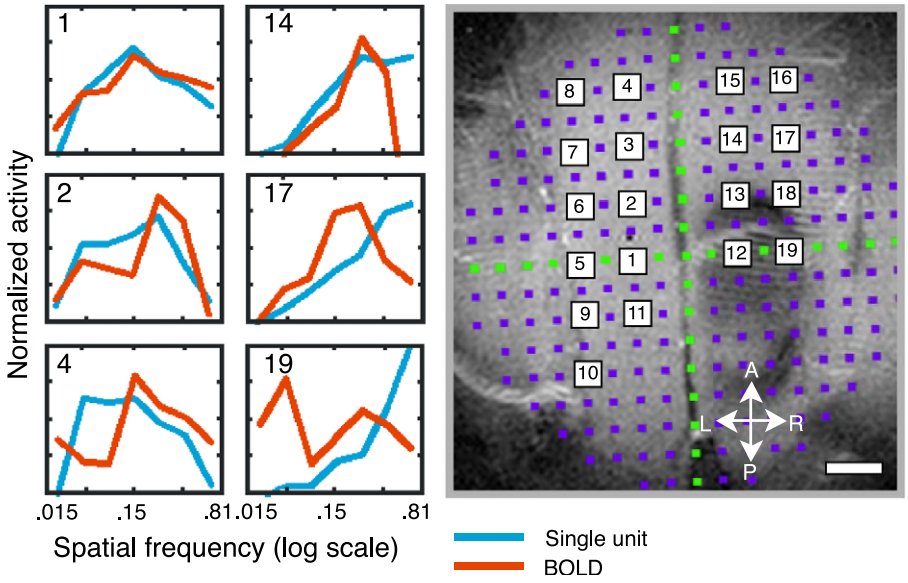

Fig. 5. Map of recording sites and sample BOLD and single-unit tuning curves in one experiment. The right panel shows a tangential image of the cat area 18 following craniotomy and chamber implantation. The blue squares indicate the positions of the Cartesian guide holes. The numbered white squares stand for guide hole positions from which single-unit responses were obtained following the MRI session (n = 19 in this animal). The plots at the left side display the tuning curves computed for the six different spatial frequencies based on single-unit (blue traces) and BOLD (red traces) responses. Numbers in the upper left corner of each plot indicate the penetration number as mapped at right. A: anterior; P: posterior; L: left; R: right. Cross is drawn at AP0 level. Spatial frequencies for the depicted tuning curves ranged from 0.81 to 0.015 cyc/deg. Scale bar: 3 mm.

plots at the left display the tuning curves computed for the six different spatial frequencies based on single-unit (blue traces) and BOLD (red traces) responses (see legend to Fig. 5 for further details). Similar experiments were performed in six different hemispheres. Notice that while all sites showed activity to at least one stimulus, single-unit tuning curves varied markedly. The results of such individual comparisons indicate that, unlike the pooled data (see Fig. 4), correlations between BOLD and single-unit responses varied markedly (e.g. compare the sites 1, 2, and 14 versus the sites 4, 17, and 19). Overall, the correlation coefficients between BOLD and single-unit response at the individual recording sites varied over an extended range ($0.0 < R^2 < 0.86$, n = 58, mean = 0.18).

Hemodynamic considerations

The data shown in Fig. 5 imply that the degree of correlation between BOLD and single-unit responses ("neuronal correspondence") might be expected to vary as a function of the voxel position across the cortex. We observed no significant correspondence between sites of high correlation and sites of high activity, either BOLD or neuronal, nor did the sites of high correlation particularly correspond with sites of large neuronal modulation. This result is consistent with the hypothesis that BOLD signals do not reflect functional architecture at the scale of orientation columns (hundreds of micrometers). Also, it is consistent with the model of the hemodynamic events during BOLD signal acquisition as depicted

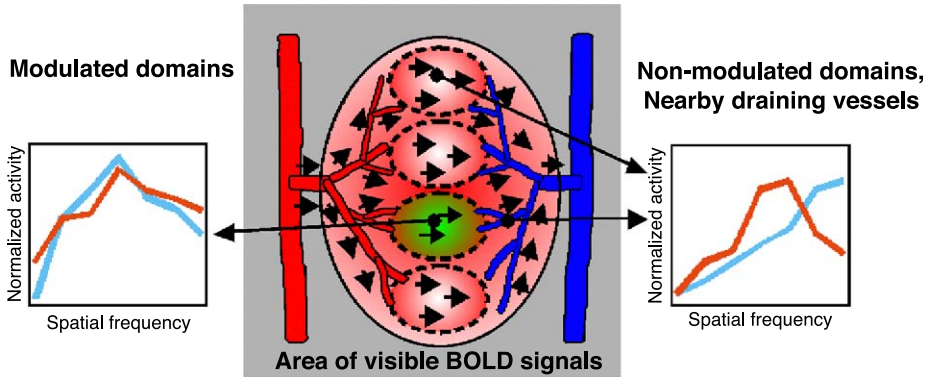

Fig. 6. Parsimonious hemodynamic events following a sensory stimulation. The central panel shows a cartoon version of the functional architecture in the visual cortex. The ellipses indicate cortical columns coding for different receptive field properties. The thick red and blue lines indicate the arterial and venous vasculature, respectively. The individual cortical columns are provided with fresh oxygenated blood through a dense network of capillaries. Red and blue traces at either side of the cartoon depict hypothetical composite tuning curves for BOLD (red) and single-unit (blue) responses. The large red ellipse in the central cartoon indicates the spread of BOLD activation beyond the site of neuronal elevation. See text for further details.

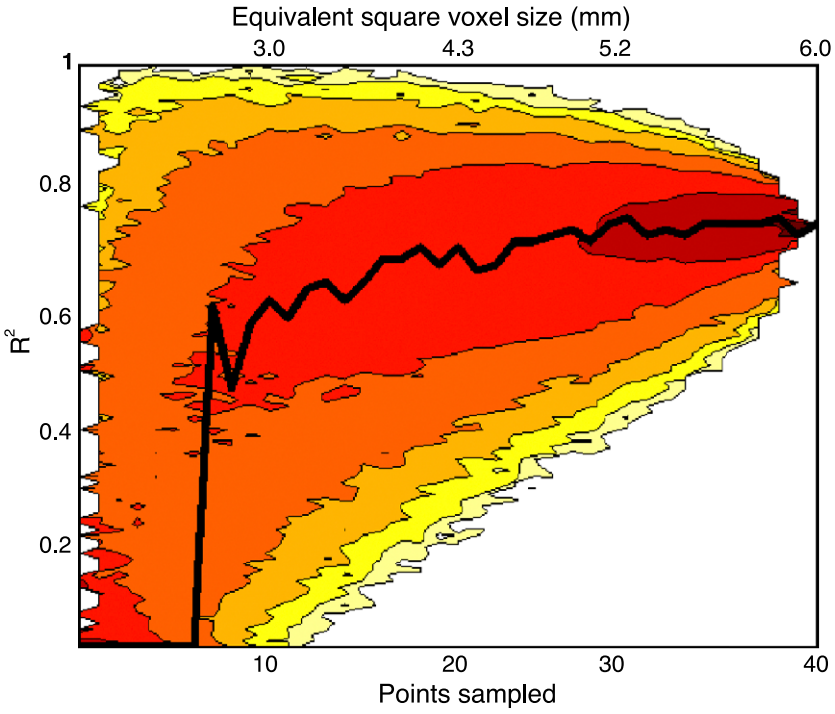

Fig. 7. Spatial correlation of BOLD and single-unit responses. The *y*-axis shows the neuronal correspondence (R^2 between BOLD and single-unit responses) as a function of the number of points sampled. Colored contours represent the probability (log scale) of obtaining a given regression coefficient between the BOLD and single-unit data as a function of the number of voxels averaged. The *x*-axis, which directly represents the number of points sampled, is also correlated with the edge length of a voxel (square root of $n \times 900$ um^2 cortical area per voxel, where n is the number of voxels) that would effectively contain an equivalent signal strength (top *x*-axis). The black line shows the peak of the distribution.

in Fig. 6. Here, the central panel displays a cartoon version of the functional architecture in the visual cortex. Ellipses indicate cortical columns coding for different receptive field properties. Thick red and blue lines indicate the arterial and venous vasculature, respectively. Individual cortical domains are provided with fresh oxygenated blood through a dense network of capillaries, and drained through the venuoles and veins indicated on the right side. Stimulation of the animal results in an increase in both the subthreshold and suprathreshold electrical activity among neurons in the respective cortical column (marked as "green" in Fig. 6). A prolonged increase in oxygen consumption follows, caused by an elevation in oxidative metabolism of active neurons (Fox and Raichle, 1986). Based on 2-deoxyglucose studies (Sokoloff et al., 1977), we can assume this increase in oxidative metabolism in cat area 18 to be co-localized with the actual site of electrical activity (Lowel et al., 1987). The increase in oxidative metabolism will elevate the local deoxyHb content in the parenchyma of active neurons, assuming there is no immediate and commensurate change in cerebral blood flow. Such transient increase of deoxyHb has been observed in recent optical spectroscopy (Malonek and Grinvald, 1996; Malonek et al., 1997), and high-field fMRI (Hu et al., 1997; Kim et al., 2000; Menon et al., 1995) studies, although controversies do still exist about its physiological origin and robustness (Buxton, 2001; Marota et al., 1999; Silva et al., 2000). This elusive nature of the "dip" may be due to the fact that the dynamics and magnitude of the dip are dependant on basal physiological condition including arterial CO_2 levels (Harel et al., 2002).

The aforementioned deoxygenation of the local cortical tissue will last only for a brief period, as oxyHb-rich blood will rush into capillaries due to increased blood flow in response to the elevated neuronal activity (Fox and Raichle, 1986). The fractional increase in blood flow exceeds the fractional elevation in $CMRO_2$ so that the local ratio of hemoglobin in blood turns in favor of oxyHb, thus resulting in a positive increase in observable BOLD MR signals despite potential increase in local blood volume. It is worth noting that oxygen-dependent signals can be measured using other, invasive techniques in anesthetized cat visual cortex, and these signals do contain structure at the level of 100 μm that can be shown to correlate with neuronal activity (Thompson et al., 2003). Thus, while anesthesia may have an effect on oxyHb signals, there is no reason to suppose that the presence of anesthetic influences prevents us from obtaining results using this preparation. Finally, it should be noted that depth of anesthesia and type of anesthesia may change the spatial coupling between blood and neural activity in significant ways, and those questions have not been explored in the present study.

In this study, we have utilized only the most commonly used positive BOLD effect for correlation with the electrophysiological data, in order for our data to be of the widest significance for comparison with conventional fMRI studies. The crucial question is: how spatially precise is the regulation of delayed hyperoxygenation of the cortical tissue? Can we assume that the vasculature system "knows" exactly which of the numerous cortical columns has been active electrically, and that only those columns will have increased blood flow and be provided with fresh oxyHb? Or alternatively, is the entire local vicinity of the active column flooded with fresh blood? If the latter scenario is true, then the delayed oxygenation signals (as detected with T_2*-based positive BOLD technique) will surpass the spatial extent of the actual activated area. Recent studies (Duong et al., 2001) indicate that the

blood flow increases are relatively but not completely specific to the active iso-orientation columns in the cat visual cortex. Cerebral blood flow (CBF) increases in the active columns were approximately 3- to 4-fold larger than CBF increases in the adjacent "nonactive" orientation domains permitting functional mapping of the iso-orientation domains using CBF-based MR imaging alone (Duong et al., 2001). However, there was also a detectable CBF increase in the nonactive columns. Thus, if we assume that $CMRO_2$ is negligible in the nonactive columns in contrast to the active columns, this can result in a large and even comparable BOLD effect over the nonactive columns as well. The area of BOLD "activation" will hence include cortical tissue areas consisting of nonactive columns (the large red area in Fig. 6). Alternatively or in addition, the spatial specificity of the BOLD response will be degraded because the deoxy/oxyhemoglobin changes that occur initially at the "active" column will not remain stationary but will propagate "downstream" in the vasculature to draining veins. Thus, BOLD signals will appear over brain tissue that is not necessarily active.

It is in this context that we can attempt to understand the marked variability in neuronal correspondence of individual recording sites. Voxels of high neuronal correspondence are presumed to be in or close to the actual site of the electrical activity (e.g. Fig. 6 cartoon). There will be a mismatch between BOLD and single-unit responses, however, if BOLD signals are obtained from voxels situated beyond the site of electrical activity, but still within the area to which the BOLD signals have spread.

Relationship between voxel size and neural correspondence

Clearly, the MRI voxel size is a key element in determining the spatial dependence of the correlation between the BOLD and electrode data. A large voxel will improve the relationship to the neuronal event, since a voxel that displays BOLD signal changes will have a much higher probability of including the site of the electrically active column when its size increases, for example, to sizes that are often used in human studies (e.g. $3 \times 3 \times 3$ mm^3). However, such a large voxel will provide only limited information about the pattern of activation due to its low spatial resolution. Smaller voxels (i.e. at the size of individual single-unit recording sites), which could potentially yield a much better spatial resolution, will result in a large variability in neuronal correspondence and the BOLD signal and a large number of "active" voxels will actually originate from positions beyond the site of electrical activity.

To quantitatively examine the spatial correspondence of the BOLD and SU signals (shown qualitatively in Fig. 5), BOLD and single-unit data pairs from individual recording sites were shuffled using methods of Monte Carlo permutation (see Materials and methods). The correspondence was calculated as a function of number of cortical points sampled. Fig. 7 shows the neuronal correspondence (R^2 between BOLD and single-unit responses) as a function of the number of points sampled. At each sample size, the distribution of correlation coefficients resulting from a large number of random shufflings is plotted on the *y*-axis. Colored contours represent the probability (log scale) of obtaining a given regression coefficient between the BOLD and single-unit data as a function of the number of voxels averaged. Each sample size effectively pools data from a certain amount of cortical area, which is shown as the second scale on the top *x*-axis. The results depicted in Fig. 7 predict that the neuronal correspondence only begins to saturate after about 8 points, which corresponds to an imaged area 2.6 mm^2. This is the smallest size at which a reasonable approximation of the maximum value of R^2 is attained (black line in Fig. 7). Furthermore, larger voxel sizes are suggested to be relatively ineffective in further improving the level of neuronal correspondence. That is, the maximum amount of variance in the underlying neuronal modulation that can be explained with the variance of T_2*-based positive BOLD is about 70%. Once the voxel size has been reduced to be smaller than approximately 2.6×2.6 mm^2, less than 50% of the variance in the underlying neuronal modulation can be explained through the observed BOLD responses.

Conclusions

In this study, we have developed a method to directly compare the BOLD and responses from multiple single-unit sites from the same cortical area. Identical stimuli were used for BOLD and single-unit studies to directly correlate the spatiotemporal coupling between the BOLD responses and the underlying neuronal activity. By taking advantage of the consecutive recording scheme, we were able to obtain correlative data from a large number of recording sites across the cat area 18.

The results of our combined BOLD and single-unit studies suggest that both local field potential (LFP) and single-unit correlate well with the BOLD signal (see Figs. 3 and 4). We have used LFP on the assumption that it represents the average activity of thousands of neurons. In agreement with previous findings (Logothetis et al., 2001), LFP signals may provide a better estimate of BOLD responses than suprathreshold spike rate. However, whether intracellular or extracellular activity is better correlated with BOLD is harder to address, since with a grating stimulus (and in fact with many types of visual stimuli) one would expect intracellular and extracellular activity to be roughly correlated with each other (Ferster, 1994; Jagadeesh et al., 1993; Nelson et al., 1994). Separating intracellular and extracellular activity would have to be accomplished using a visual stimulus known to do so. For example, one could look at spatial activity resulting from the edge of a visual stimulus (Grinvald et al., 1994; Gulyas et al., 1987; Knierim and van Essen, 1992). Since 'extra-classical' receptive fields by definition reflect intracellular activity, it follows that a stimulus with an edge creates regions of cortex where activity is only intracellular in origin. Optical imaging studies (Grinvald et al., 1994; Toth et al., 1996) have concluded that intracellular activity does contribute to the optical signal, suggesting that it might contribute to the BOLD signal as well. One imaging experiment presumptively showing a large contribution of intracellular activity to the optical imaging signal uses focal iontophoresis of GABA-A antagonist bicuculline methiodide (Ajima et al., 1999; Toth et al., 1997) to generate a mismatch between intracellular and extracellular activity. This is a rare case where a blood-dependent signal could be reversibly altered by an artificial manipulation of neural activity. We are currently repeating these studies using fMRI techniques to elucidate the spatial contribution of the intracellular and extracellular activity in BOLD functional MRI signals.

Our results are consistent with and extend those of Logothetis et al. (2001). In line with their study, we also found an approximated linear coupling between BOLD and neuronal activity if a relatively large activity area is considered. Together with previous studies by other groups (Heeger et al., 2000; Rees et al., 2000), these results suggest that the functional "activation" areas identi-

fied in the published BOLD studies with relatively large voxel sizes of around 3–5 mm^2 may indeed accurately reflect the underlying neuronal activity. The results of our study also suggest, however, that such linear coupling cannot assumed to be always valid. While we do not suggest the following numbers to be inviolable or universal across different species and cortical areas, our data indicate that in cat area 18, only less than 50% of the variance in neuronal modulation during stimulation with simple moving gratings can effectively be accounted for based on observed BOLD modulation if a voxel size of less than 2.6 × 2.6 mm^2 or smaller is used. Voxels of sub-millimeter scale, therefore, will have to be interpreted with great caution. Therefore, sub-millimeter resolution fMRI imaging would seem to call for the mapping of MR signal sources other than T_2*-based BOLD contrast. In recent studies, both the use of the "initial dip" (Kim et al., 2000) and CBF (Duong et al., 2001) contrast for functional image construction have been suggested to yield foci of activity at a sub-millimeter columnar resolution. Methods of active suppression of large draining vessel components, such as spin-echo techniques in conjunction with the use of ultra-high-field MRI scanners (Lee et al., 1999; Ugurbil et al., 1999), are also imaginable as a means to limit the spread of hemodynamic activity beyond the site of neuronal activity. The methods described in this study can also be applied to relate such nonconventional fMRI techniques to the underlying neuronal modulation.

Acknowledgments

We thank Drs. T. Duong and N. Harel for their assistance during some of the initial experiments. N. Port from NIH provided the initial recording chambers for testing. This work was supported by the NIH (MH57180, MH67530, NS38295, RR08079), the W.M. Keck Foundation, and the Whitaker Foundation, NARSAD.

References

Ajima, A., Matsuda, Y., Ohki, K., Kim, D.S., Tanaka, S., 1999. GABA-mediated representation of temporal information in rat barrel cortex. NeuroReport 10, 1973–1979.

Attwell, D., Iadecola, C., 2002. The neural basis of functional brain imaging signals. Trends Neurosci. 25, 621–625.

Bandettini, P.A., Wong, E.C., Hinks, R.S., Tikofsky, R.S., Hyde, J.S., 1992. Time course EPI of human brain function during task activation. Magn. Reson. Med. 25, 390–397.

Buxton, R.B., 2001. The elusive initial dip. NeuroImage 13, 953–958.

Duong, T.Q., Kim, D.S., Ugurbil, K., Kim, S.G., 2001. Localized cerebral blood flow response at submillimeter columnar resolution. Proc. Natl. Acad. Sci. U. S. A. 98, 10904–10909.

Engel, S.A., Rumelhart, D.E., Wandell, B.A., Lee, A.T., Glover, G.H., Chichilnisky, E.J., Shadlen, M.N., 1994. fMRI of human visual cortex. Nature 369, 525.

Ferster, D., 1994. Linearity of synaptic interactions in the assembly of receptive fields in cat visual cortex. Curr. Opin. Neurobiol. 4, 563–568.

Fox, P.T., Raichle, M.E., 1986. Focal physiological uncoupling of cerebral blood flow and oxidative metabolism during somatosensory stimulation in human subjects. Proc. Natl. Acad. Sci. U. S. A. 83, 1140–1144.

Grinvald, A., Lieke, E.E., Frostig, R.D., Hildesheim, R., 1994. Cortical point-spread function and long-range lateral interactions revealed by real-time optical imaging of macaque monkey primary visual cortex. J. Neurosci. 14, 2545–2568.

Gulyas, B., Orban, G.A., Duysens, J., Maes, H., 1987. The suppressive influence of moving textured backgrounds on responses of cat striate neurons to moving bars. J. Neurophysiol. 57, 1767–1791.

Harel, N., Lee, S.P., Nagaoka, T., Kim, D.S., Kim, S.G., 2002. Origin of negative blood oxygenation level-dependent fMRI signals. J. Cereb. Blood Flow Metab. 22, 908–917.

Heeger, D.J., Huk, A.C., Geisler, W.S., Albrecht, D.G., 2000. Spikes versus BOLD: what does neuroimaging tell us about neuronal activity? Nat. Neurosci. 3, 631–633.

Hu, X., Le, T.H., Ugurbil, K., 1997. Evaluation of the early response in fMRI in individual subjects using short stimulus duration. Magn. Reson. Med. 37, 877–884.

Hubel, D., Wiesel, T.N., 1962. Receptive field, binocular interaction and functional architecture in the cat's visual cortex. J. Physiol. (London) 160, 106–154.

Hubener, M., Shoham, D., Grinvald, A., Bonhoeffer, T., 1997. Spatial relationships among three columnar systems in cat area 17. J. Neurosci. 17, 9270–9284.

Issa, N.P., Trepel, C., Stryker, M.P., 2000. Spatial frequency maps in cat visual cortex. J. Neurosci. 20, 8504–8514.

Jagadeesh, B., Wheat, H.S., Ferster, D., 1993. Linearity of summation of synaptic potentials underlying direction selectivity in simple cells of the cat visual cortex. Science 262, 1901–1904.

Kim, S.G., Ashe, J., Georgopoulos, A.P., Merkle, H., Ellermann, J.M., Menon, R.S., Ogawa, S., Ugurbil, K., 1993. Functional imaging of human motor cortex at high magnetic field. J. Neurophysiol. 69, 297–302.

Kim, D.S., Duong, T.Q., Kim, S.G., 2000. High-resolution mapping of iso-orientation columns by fMRI. Nat. Neurosci. 3, 164–169.

Knierim, J.J., van Essen, D.C., 1992. Neuronal responses to static texture patterns in area V1 of the alert macaque monkey. J. Neurophysiol. 67, 961–980.

Kwong, K.K., Belliveau, J.W., Chesler, D.A., Goldberg, I.E., Weisskoff, R.M., Poncelet, B.P., Kennedy, D.N., Hoppel, B.E., Cohen, M.S., Turner, R., et al., 1992. Dynamic magnetic resonance imaging of human brain activity during primary sensory stimulation. Proc. Natl. Acad. Sci. U. S. A. 89, 5675–5679.

Lee, S.P., Silva, A.C., Ugurbil, K., Kim, S.G., 1999. Diffusion-weighted spin-echo fMRI at 9.4 T: microvascular/tissue contribution to BOLD signal changes. Magn. Reson. Med. 42, 919–928.

Logothetis, N.K., Pauls, J., Augath, M., Trinath, T., Oeltermann, A., 2001. Neurophysiological investigation of the basis of the fMRI signal. Nature 412, 150–157.

Lowel, S., Freeman, B., Singer, W., 1987. Topographic organization of the orientation column system in large flat-mounts of the cat visual cortex: a 2-deoxyglucose study. J. Comp. Neurol. 255, 401–415.

Maffei, L., Fiorentini, A., 1977. Spatial frequency rows in the striate visual cortex. Vision Res. 17, 257–264.

Malonek, D., Grinvald, A., 1996. Interactions between electrical activity and cortical microcirculation revealed by imaging spectroscopy: implications for functional brain mapping. Science 272, 551–554.

Malonek, D., Dirnagl, U., Lindauer, U., Yamada, K., Kanno, I., Grinvald, A., 1997. Vascular imprints of neuronal activity: relationships between the dynamics of cortical blood flow, oxygenation, and volume changes following sensory stimulation. Proc. Natl. Acad. Sci. U. S. A. 94, 14826–14831.

Marota, J.J., Ayata, C., Moskowitz, M.A., Weisskoff, R.M., Rosen, B.R., Mandeville, J.B., 1999. Investigation of the early response to rat forepaw stimulation. Magn. Reson. Med. 41, 247–252.

Menon, R.S., Ogawa, S., Hu, X., Strupp, J.P., Anderson, P., Ugurbil, K., 1995. BOLD based functional MRI at 4 Tesla includes a capillary bed contribution: echo-planar imaging correlates with previous optical imaging using intrinsic signals. Magn. Reson. Med. 33, 453–459.

Movshon, J.A., Thompson, I.D., Tolhurst, D.J., 1978. Spatial and temporal contrast sensitivity of neurones in areas 17 and 18 of the cat's visual cortex. J. Physiol. 283, 101–120.

Nelson, S., Toth, L., Sheth, B., Sur, M., 1994. Orientation selectivity of cortical neurons during intracellular blockade of inhibition. Science 265, 774–777.

Ogawa, S., Tank, D.W., Menon, R., Ellermann, J.M., Kim, S.G., Merkle, H., Ugurbil, K., 1992. Intrinsic signal changes accompanying sensory stimulation: functional brain mapping with magnetic resonance imaging. Proc. Natl. Acad. Sci. U. S. A. 89, 5951–5955.

Ogawa, S., Lee, T.M., Stepnoski, R., Chen, W., Zhu, X.H., Ugurbil, K., 2000. An approach to probe some neural systems interaction by functional MRI at neural time scale down to milliseconds. Proc. Natl. Acad. Sci. U. S. A. 97, 11026–11031.

Rees, G., Friston, K., Koch, C., 2000. A direct quantitative relationship between the functional properties of human and macaque V5. Nat. Neurosci. 3, 716–723.

Shadlen, M.N., Newsome, W.T., 1994. Noise, neural codes and cortical organization. Curr. Opin. Neurobiol. 4, 569–579.

Silva, A.C., Lee, S.P., Iadecola, C., Kim, S.G., 2000. Early temporal characteristics of cerebral blood flow and deoxyhemoglobin changes during somatosensory stimulation. J. Cereb. Blood Flow Metab. 20, 201–206.

Singer, W., 1999. Time as coding space? Curr. Opin. Neurobiol. 9, 189–194.

Sokoloff, L., Reivich, M., Kennedy, C., Des Rosiers, M.H., Patlak, C.S., Pettigrew, K.D., Sakurada, O., Shinohara, M., 1977. The [14C]deoxyglucose method for the measurement of local cerebral glucose utilization: theory, procedure, and normal values in the conscious and anesthetized albino rat. J. Neurochem. 28, 897–916.

Thompson, J.K., Peterson, M.R., Freeman, R.D., 2003. Single-neuron activity and tissue oxygenation in the cerebral cortex. Science 299, 1070–1072.

Toth, L.J., Rao, S.C., Kim, D.S., Somers, D., Sur, M., 1996. Subthreshold facilitation and suppression in primary visual cortex revealed by intrinsic signal imaging. Proc. Natl. Acad. Sci. U. S. A. 93, 9869–9874.

Toth, L.J., Kim, D.S., Rao, S.C., Sur, M., 1997. Integration of local inputs in visual cortex. Cereb. Cortex 7, 703–710.

Ugurbil, K., Hu, X., Chen, W., Zhu, X.H., Kim, S.G., Georgopoulos, A., 1999. Functional mapping in the human brain using high magnetic fields. Philos. Trans. R. Soc. London, B. Biol. Sci. 354, 1195–1213.

Ugurbil, K., Toth, L., Kim, D.S., 2003. How accurate is magnetic resonance imaging of brain function? Trends Neurosci. 26, 108–114.

Wagner, A.D., Schacter, D.L., Rotte, M., Koutstaal, W., Maril, A., Dale, A.M., Rosen, B.R., Buckner, R.L., 1998. Building memories: remembering and forgetting of verbal experiences as predicted by brain activity. Science 281, 1188–1191.